Do different turbid media with matched bulk optical properties also exhibit similar polarization properties?

Manzoor Ahmad,[1,2] Sanaz Alali,[1,*] Anthony Kim, [1] Michael F. G. Wood,[1] Masroor Ikram,[2] and I. Alex Vitkin[1]

[1]*Division of Biophysics and Bioimaging, Ontario Cancer Institute/University Health Network and Department of Medical Biophysics, University of Toronto, 610 University Avenue, Toronto, Ontario M5G 2M9, Canada*
[2]*Department of Physics and Applied Mathematics, Pakistan Institute of Engineering and Applied Sciences, Islamabad 45650, Pakistan*
**sanaz.alali@utoronto.ca*

Abstract: We here investigate polarimetric behavior of thick samples of porcine liver, Intralipid, and microsphere-based tissue phantoms whose absorption and scattering properties are matched. Using polarized light we measured reflection mode Mueller matrices and derived linear/circular/total depolarization rates, based on polar decomposition. According to our results, phantoms exhibit greater depolarization rates in the backscattering geometry than the liver sample. The enhanced tissue polarization preservation differs from previous reports of polarimetric transmission studies, with the likely cause of this difference being the angular dependence of the single-scattering phase function. Also, Intralipid approximated polarimetric liver behavior well, whereas the polystyrene phantoms did not.

OCIS codes: (170.3660) Light propagation in tissues; (110.0113) Imaging through turbid media; (290.5855) Scattering, polarization; (290.4020) Mie theory

References and links

1. J. R. Mourant, T. M. Johnson, S. Carpenter, A. Guerra, T. Aida, and J. P. Freyer, "Polarized angular dependent spectroscopy of epithelial cells and epithelial cell nuclei to determine the size scale of scattering structures," J. Biomed. Opt. **7**(3), 378–387 (2002).
2. S. L. Jacques, J. R. Roman, and K. Lee, "Imaging superficial tissues with polarized light," Lasers Surg. Med. **26**(2), 119–129 (2000).
3. M. F. G. Wood, N. Ghosh, M. A. Wallenburg, S. H. Li, R. D. Weisel, B. C. Wilson, R. K. Li, and I. A. Vitkin, "Polarization birefringence measurements for characterizing the myocardium, including healthy, infarcted, and stem-cell-regenerated tissues," J. Biomed. Opt. **15**(4), 047009 (2010).
4. S. L. Jacques, R. Samatham, S. Isenhath, and K. Lee, "Polarized light camera to guide surgical excision of skin cancers," Proc. SPIE **6842**, 68420I (2008).
5. X. Wang and L. V. Wang, "Propagation of polarized light in birefringent turbid media: a Monte Carlo study," J. Biomed. Opt. **7**(3), 279–290 (2002).
6. M. F. G. Wood, X. Guo, and I. A. Vitkin, "Polarized light propagation in multiply scattering media exhibiting both linear birefringence and optical activity: Monte Carlo model and experimental methodology," J. Biomed. Opt. **12**(1), 014029 (2007).
7. N. Ghosh, M. F. G. Wood, and I. A. Vitkin, "Mueller matrix decomposition for extraction of individual polarization parameters from complex turbid media exhibiting multiple scattering, optical activity, and linear birefringence," J. Biomed. Opt. **13**(4), 044036 (2008).
8. N. Ghosh, M. F. G. Wood, and I. A. Vitkin, "Polarimetry in turbid, birefringent, optically active media: a Monte Carlo study of Mueller matrix decomposition in the backscattering geometry," J. Appl. Phys. **105**(10), 102023 (2009).
9. P. Shukla, A. Awasthi, P. K. Pandey, and A. Pradhan, "Discrimination of normal and dysplasia in cervix tissue by Mueller matrix analysis," Proc. SPIE **6864**, 686417 (2008).
10. J. C. Ramella-Roman and D. D. Duncan, "A new approach to Mueller matrix reconstruction of skin cancer lesions using a dual rotating retarder polarimeter," Proc. SPIE **6080**, 60800M (2006).

#154276 - $15.00 USD Received 7 Sep 2011; revised 5 Oct 2011; accepted 6 Oct 2011; published 4 Nov 2011

11. M. R. Antonelli, A. Pierangelo, T. Novikova, P. Validire, A. Benali, B. Gayet, and A. De Martino, "Mueller matrix imaging of human colon tissue for cancer diagnostics: how Monte Carlo modeling can help in the interpretation of experimental data," Opt. Express **18**(10), 10200–10208 (2010).
12. B. D. Cameron and H. Anumula, "Development of a real-time corneal birefringence compensated glucose sensing polarimeter," Diabetes Technol. Ther. **8**(2), 156–164 (2006).
13. G. L. Coté, M. D. Fox, and R. B. Northrop, "Noninvasive optical polarimetric glucose sensing using a true phase measurement technique," IEEE Trans. Biomed. Eng. **39**(7), 752–756 (1992).
14. M. F. G. Wood, N. Ghosh, X. Guo, and I. A. Vitkin, "Toward noninvasive glucose sensing using polarization analysis of multiply scattered light," in *Handbook of Optical Sensing of Gloucose in Biological Fluids and Tissues*, V. V. Tuchin, ed. (CRC Press, 2008), pp. 527–558
15. J. M. Schmitt, A. H. Gandjbakhche, and R. F. Bonner, "Use of polarized light to discriminate short-path photons in a multiply scattering medium," Appl. Opt. **31**(30), 6535–6546 (1992).
16. D. Bicout, C. Brosseau, A. S. Martinez, and J. M. Schmitt, "Depolarization of multiply scattered waves by spherical diffusers: Influence of the size parameter," Phys. Rev. E Stat. Phys. Plasmas Fluids Relat. Interdiscip. Topics **49**(2), 1767–1770 (1994).
17. A. D. Kim and M. Moscoso, "Influence of the relative refractive index on the depolarization of multiply scattered waves," Phys. Rev. E Stat. Nonlin. Soft Matter Phys. **64**(2), 026612 (2001).
18. N. Ghosh, A. Pradhan, P. K. Gupta, S. Gupta, V. Jaiswal, and R. P. Singh, "Depolarization of light in a multiply scattering medium: effect of the refractive index of a scatterer," Phys. Rev. E Stat. Nonlin. Soft Matter Phys. **70**(6), 066607 (2004).
19. N. Ghosh, P. K. Gupta, A. Pradhan, and S. K. Majumder, "Anomalous behavior of depolarization of light in a turbid medium," Phys. Lett. A **354**(3), 236–242 (2006).
20. X. Guo, M. F. G. Wood, N. Ghosh, and I. A. Vitkin, "Depolarization of light in turbid media: a scattering event resolved Monte Carlo study," Appl. Opt. **49**(2), 153–162 (2010).
21. V. Sankaran, M. J. Everett, D. J. Maitland, and J. T. Walsh, Jr., "Comparison of polarized-light propagation in biological tissue and phantoms," Opt. Lett. **24**(15), 1044–1046 (1999).
22. V. Sankaran, J. T. Walsh, Jr., and D. J. Maitland, "Polarized light propagation through tissue phantoms containing densely packed scatterers," Opt. Lett. **25**(4), 239–241 (2000).
23. V. Sankaran, K. Schönenberger, J. T. Walsh, Jr., and D. J. Maitland, "Polarization discrimination of coherently propagating light in turbid media," Appl. Opt. **38**(19), 4252–4261 (1999).
24. N. Ghosh, P. K. Gupta, H. S. Patel, B. Jain, and B. N. Singh, "Depolarization of light in tissue phantoms –effect of collection geometry," Opt. Commun. **222**(1-6), 93–100 (2003).
25. V. Sankaran, J. T. Walsh, Jr., and D. J. Maitland, "Comparative study of polarized light propagation in biologic tissues," J. Biomed. Opt. **7**(3), 300–306 (2002).
26. A. Kim, M. Roy, F. Dadani, and B. C. Wilson, "A fiberoptic reflectance probe with multiple source-collector separations to increase the dynamic range of derived tissue optical absorption and scattering coefficients," Opt. Express **18**(6), 5580–5594 (2010).
27. T. J. Farrell, M. S. Patterson, and B. C. Wilson, "A diffusion theory model of spatially resolved, steady-state diffuse reflectance for the noninvasive determination of tissue optical properties in vivo," Med. Phys. **19**(4), 879–888 (1992).
28. C. Brosseau, *Fundamentals of Polarized Light: A Statistical Optics Approach* (Wiley, NewYork,1998).
29. M. A. Wallenburg, M. Pop, M. F. G. Wood, N. Ghosh, G. A. Wright, and I. A. Vitkin, "Comparison of optical polarimetry and diffusion tensor MR imaging for assessing myocardial anisotropy," J. Innovative Opt. Health Sci. **3**(2), 109–121 (2010).
30. S. Manhas, M. K. Swami, P. Buddhiwant, N. Ghosh, P. K. Gupta, and J. Singh, "Mueller matrix approach for determination of optical rotation in chiral turbid media in backscattering geometry," Opt. Express **14**(1), 190–202 (2006).
31. N. Ghosh, M. F. G. Wood, S. H. Li, R. D. Weisel, B. C. Wilson, R. K. Li, and I. A. Vitkin, "Mueller matrix decomposition for polarized light assessment of biological tissues," J Biophotonics **2**(3), 145–156 (2009).
32. X. Li and G. Yao, "Mueller matrix decomposition of diffuse reflectance imaging in skeletal muscle," Appl. Opt. **48**(14), 2625–2631 (2009).
33. N. Ghosh, M. F. G. Wood, and I. A. Vitkin, "Influence of the order of the constituent basis matrices on the Mueller matrix decomposition-derived polarization parameters in complex turbid media such as biological tissues," Opt. Commun. **283**(6), 1200–1208 (2010).
34. S. Lu and R. A. Chipman, "Interpretation of Mueller matrices based on polar decomposition," J. Opt. Soc. Am. A **13**(5), 1106–1113 (1996).
35. S. Alali, M. Ahmad, A. Kim, N. Vurgun, M. F. G. Wood, and I. A. Vitkin, "Depolarization of light in tissues of varying optical properties: a comparative study," PLoS ONE ((submitted to).
36. J.-P. Ritz, A. Roggan, C. Isbert, G. Müller, H. J. Buhr, and C. T. Germer, "Optical properties of native and coagulated porcine liver tissue between 400 and 2400 nm," Lasers Surg. Med. **29**(3), 205–212 (2001).
37. H. J. van Staveren, C. J. M. Moes, J. van Marie, S. A. Prahl, and M. J. C. van Gemert, "Light scattering in Intralipid-10% in the wavelength range of 400-1100 nm," Appl. Opt. **30**(31), 4507–4514 (1991).
38. J. M. Schmitt and G. Kumar, "Optical scattering properties of soft tissue: a discrete particle model," Appl. Opt. **37**(13), 2788–2797 (1998).

#154276 - $15.00 USD Received 7 Sep 2011; revised 5 Oct 2011; accepted 6 Oct 2011; published 4 Nov 2011

39. J. R. Mourant, J. P. Freyer, A. H. Hielscher, A. A. Eick, D. Shen, and T. M. Johnson, "Mechanisms of light scattering from biological cells relevant to noninvasive optical-tissue diagnostics," Appl. Opt. **37**(16), 3586–3593 (1998).
40. J. Beuthan, O. Minet, J. Helfmann, M. Herrig, and G. Müller, "The spatial variation of the refractive index in biological cells," Phys. Med. Biol. **41**(3), 369–382 (1996).
41. H. C. V. de Hulst, *Light Scattering by Small Particles* (Dover, New York, 1981)
42. R. Graaff, J. G. Aarnoudse, F. F. M. de Mul, and H. W. Jentink, "Light propagation parameters for anisotropically scattering media based on a rigorous solution of the transport equation," Appl. Opt. **28**(12), 2273–2279 (1989).
43. L. O. Reynolds and N. J. McCormick, "Approximation two parameter phase function for light scattering," J. Opt. Soc. Am. **70**(10), 1206–1212 (1980).

1. Introduction

In the field of optical bio-diagnostics, tissue polarization imaging offers the potential of improved contrast by partially rejecting highly scattered from unscattered or weakly scattered photons [1,2]. In addition to imaging, it has been demonstrated that several interesting polarimetric properties of turbid media can be useful for tissue characterization [2–8]. For example, polarized light is sensitive to morphological tissue micro-architecture, with preliminary demonstrations of early cancerous detection [4,9–11], and anisotropy assessment of birefringent tissues in healthy, infracted and stem-cell-regenerated cardiac models [8,9]. Polarimetric sensitivity to tissue composition has also been explored, primarily in the context of potential non-invasive glucose sensing in diabetic patients [12–14].

Several studies of polarized light propagation in turbid medium like biological tissues, both experimental and theoretical, have been carried out. Owing to the extreme complexity of biological tissues, one often resorts to simpler tissue phantoms such as Intralipid suspensions or microspheres-in-water colloids, for controlled measurements and for theoretical simulations. For example, to calibrate any polarization measurement system or to test polarization-derived metrics, phantoms with known optical properties and polarimetric behavior are useful [6–8,11]. The calibrated system and those metrics can then be utilized to characterize arbitrary biological tissues. While these simpler formulations can mimic tissues well with respect to intensity-based optical metrics (absorption and scattering coefficients, anisotropy of scattering, light fluence, diffuse reflectance, etc.), the situation is more complicated when light polarization properties are considered. Depolarization mechanisms are different for different incident light polarization states, and are sensitively dependent on the details of the refractive index variation of the scattering media, even for otherwise comparable optical properties (absorption and scattering coefficients and scattering anisotropy) [15–20]. Given the different nature of scattering in tissues and in scattering phantom suspensions, it is not surprising that previous studies specifically aimed at comparing polarized light propagation in tissues and in matched tissue phantoms have reported differences. For example, significant variations in polarized light transmission through thin slabs of biological tissues and optical-properties-matched tissue phantoms were observed [21–24]. In general, tissues in thin-sample transmission geometry were seen to be more depolarizing than phantoms for both linear and circular polarization states, an effect tentatively attributed to dependent scattering mechanisms [21–24]. Moreover, circular depolarization was observed to be higher than linear depolarization in different tissues expect blood [21,25]. However, systematic polarimetric comparisons of tissues and different types of matched tissue phantoms, that also investigate the significant influence of measurement geometry (e.g., reflection from a thick slab, geometry of significant clinical interest), have not been reported.

In this work, we have studied the polarization properties of thick samples of biological tissue (porcine liver) and different phantoms in reflection geometry. We measured the optical properties of liver, then fabricated phantoms with tissue-matched absorption coefficients (via addition of Naphthol Green dye) and scattering properties (scattering or reduced scattering coefficient, using Intralipid suspensions and polystyrene microspheres). Mueller-matrix

#154276 - $15.00 USD Received 7 Sep 2011; revised 5 Oct 2011; accepted 6 Oct 2011; published 4 Nov 2011

measurements were then performed on tissue and phantom samples, and depolarization rates were extracted using polar matrix decomposition. Interesting differences in linear and circular depolarization rates were observed, with the general trend of greater depolarization in phantoms than in porcine liver. These reflection-mode findings are in contrast to previously reported trends in thin-sample transmission, where the phantoms exhibited greater polarization retention. This underscores the importance of detection geometry and of systematic polarimetric studies for potential tissue characterization and imaging applications.

2. Materials and methods

2.1. Optical properties measurement system

Prior to measuring the polarization properties of liver and its optically-matched phantoms, optical properties of all samples were measured. A fiber-based reflectance probe (using fiber optics with numerical aperture of 0.22 and core diameter of 200 μm) with multiple source-collector separations based on spatially resolved diffuse reflectance measurements was used [26,27]. Briefly, the system consists of an optical multiplexer (Model MPM-2000, Ocean Optics, Dunedin, FL, USA) for input and output light signals. For light source, diode laser (Thorlabs, Newton, NJ, USA) at 635 nm was coupled to the input port of optical multiplexer. Reflected light detected via the each pick-up probe fibers (0.8, 1.5, 2.4, 4.0 and 5.3 mm distance from the incident source fiber) was coupled to the output ports of the multiplexer, and then routed to the photodetector (Ocean Optics Spectrometer, Model S2000). Reflectance as a function of radial distance data thus collected was processed via diffusion theory to yield the sample absorption and reduced scattering coefficients, assuming homogeneous optical properties in the volume of light interrogation [27]. Prior to, and between all reported measurements, system stability was ensured with calibration measurements on a control phantom with known scattering and absorption properties.

2.2. Mueller matrix polarimetry imaging system

Figure 1 shows a schematic of the polarimetric imaging system used for these experiments. Diode laser (Thorlabs, Newton, New Jersey) at a wavelength of 635 nm was used to seed the system. The polarizer P1 generated different incident linearly polarized states. For circularly polarized light incidence, removable quarter-wave plate QWP1 was placed after the polarizer. In order to illuminate the sample with light spot of 7 mm diameter, lens L1 was placed before the sample. After interacting with sample, which was placed in a $1\text{cm} \times 1\text{cm} \times 4\text{cm}$ quartz cuvette, a fraction of the backscattered light at an angle of 25° with the incident beam was collected by a quarter-wave plate QWP2 and a linear analyzer P2. Lens L2 then focused the light onto the 1.5×1.5 cm^2 photoreceptor of a charge-coupled device camera (CoolSNAPK4,

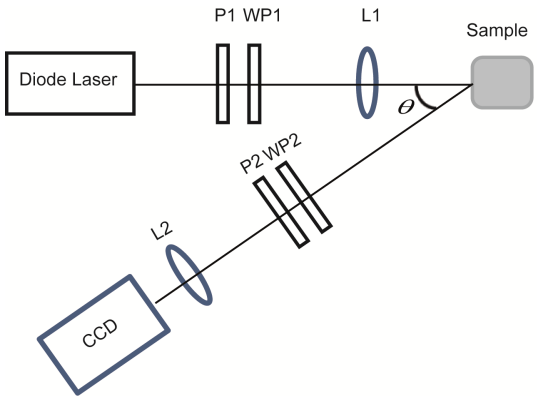

Fig. 1. Schematic diagram of polarimetric imaging system. P1 and P2 are polarizers; QWP1 and QWP2 are removable quarter-wave plates; L1 and L2 are lenses, the angle θ is 25 degrees.

#154276 - $15.00 USD Received 7 Sep 2011; revised 5 Oct 2011; accepted 6 Oct 2011; published 4 Nov 2011

Photometrics, Tucson, Arizona). The CCD viewed approximately 1.5×1.5 cm^2 square with the optical illumination on the cuvette in its center.

The polarization transfer function of the medium, known as Mueller matrix, can be calculated from a total of 24 polarization reflectance images [28]. In this approach [28,29], four different incident polarization states were generated (linear horizontal (*H*), linear vertical (*V*), linear + 45° (*P*) and right circularly polarized state (*R*)). After interacting with the sample, six different output states for each of the four different inputs were measured: four states same as input, plus linear –45° (*B*) and left circularly (*L*) polarized states. Mueller matrix images were calculated from these 24 raw images by

$$M = \begin{bmatrix} m_{11} & m_{12} & m_{13} & m_{14} \\ m_{21} & m_{22} & m_{23} & m_{24} \\ m_{31} & m_{32} & m_{33} & m_{34} \\ m_{41} & m_{42} & m_{43} & m_{44} \end{bmatrix}$$

$$= \frac{1}{4} \begin{bmatrix} HH+HV+VH+VV & HH+HV-VH-VV & 2(PH+PV)-4m_{11} & 2(RH+RV)-4m_{11} \\ HH-HV+VH-VV & HH-HV-VH+VV & 2(PH-PV)-4m_{21} & 2(RH-RV)-4m_{21} \\ HP-HB-VP-VB & HP-HB-VP+VB & 2(PP-PB)-4m_{31} & 2(RP-RB)-4m_{31} \\ HR-HL+VR-VL & HR-HL-HR+VL & 2(PR-PL)-4m_{41} & 2(RR-RL)-4m_{41} \end{bmatrix} \quad (1)$$

where each measurement is denoted by two letters. The first letter represents the incident polarization state, and the second denotes the analyzing optics orientation. For example, *HV* means an image resulting from incident horizontally polarized light detected through a vertical linear polarizer in front of the CCD. Note that for this detection geometry, there are no specular reflection effects, thus enhancing sensitivity to bulk sample polarization properties.

2.3. Mueller matrix decomposition

All the polarimetric properties of the material under study are folded in the measured Mueller matrix in a complex and inter-related way. This complicates their independent extraction and hinders results interpretation. In case of biological tissues, the simultaneously-occurring important polarization properties include depolarization, birefringence and optical activity [8,29–33]. In order to separate these effects and quantify them (we are interested in depolarization in this study), the Lu and Chipman decomposition procedure [34] has been developed and adapted for tissue polarimetry studies [7,8,29–33]. In this approach the Mueller matrix is decomposed into the product of three constituent 'basis' matrices: a diattenuator matrix M_D, a retarder matrix M_R, and a depolarizer matrix M_Δ. Mathematically, this can be written as

$$M = M_\Delta M_R M_D \quad (2)$$

As matrix multiplication is order-dependent (non-communitive), other multiplication sequences in Eq. (2) are possible. However, we have recently shown that product in Eq. (2), or its reverse order, always leads to physically realizable Mueller matrix [33,34]. In the current study, we are focusing on the physically measurable effects of depolarization contained in the depolarizer submatrix M_Δ. The depolarizer matrix can be written as [34]

$$M_\Delta = \begin{bmatrix} 1 & \vec{0}^T \\ \vec{P}_\Delta & m_\Delta \end{bmatrix} \quad (3)$$

where $\vec{0}_T$ is 3×1 null vector, $\vec{P}_\Delta$ is 3×1 polarizance vector, and m_Δ is 3×3 submatrix of

#154276 - $15.00 USD Received 7 Sep 2011; revised 5 Oct 2011; accepted 6 Oct 2011; published 4 Nov 2011

M_Δ. Total depolarization Δ_T (depolarization power) can be defined as [7,34,35]

$$\Delta_T = 1 - \frac{|m_\Delta(1,1)| + |m_\Delta(2,2)| + |m_\Delta(3,3)|}{3} \quad (4)$$

We proceed further and define linear and circular depolarizations Δ_L and Δ_C as

$$\Delta_L = 1 - \frac{|m_\Delta(1,1)| + |m_\Delta(2,2)|}{2} \quad (5)$$

and

$$\Delta_C = 1 - |m_\Delta(3,3)| \quad (6)$$

To clarify this formalism, note that these metrics refer to the intrinsic depolarization properties *of the sample* in a particular imaging geometry and, should not to be confused with the various degrees of polarizations *of the light*, derivable from the Stokes vectors. The two types of descriptors can be related to each other, but the details need not concern us here. A separate forthcoming publication discusses these issues further [35].

2.4. Sample preparation

Porcine liver and four different phantoms composed of Intralipid and of monodispersed polystyrene microspheres in water, with optical properties matched to liver, were investigated in this study. Liver was obtained from a local abattoir within 3 hours of animal sacrifice. Optical properties of the liver were measured by the system described in section 2.1, yielding the absorption coefficient μ_a and reduced scattering coefficient μ_s'. Scattering coefficient μ_s and reduced scattering coefficient μ_s' are related by the expression $\mu_s' = (1-g)\mu_s$, where g is anisotropy factor. The compositions of the phantoms were then adjusted by quantitative dilutions of its absorption (Naphthol Green) and scattering constituents (Intralipid or polystyrene microspheres) to match the liver coefficients. The optical properties of the liver and phantoms are presented in Table 1. We prepared three different phantoms matched with the μ_a and μ_s' of the porcine liver: Intralipid phantom IL, 1-μm-diam PS phantom 1, and 1.4-μm-diam PS phantom 2; one additional 1.4-μm-diam PS phantom 3 was prepared to match μ_a and μ_s (versus μ_s') of the liver.

Table 1. Summary of the optical properties of porcine liver and turbid phantoms suspensions[a]

Sample	d	μ_a	μ_s'	g	μ_s
Porcine Liver	—	4.14 cm^{-1}	6.96 cm^{-1}	0.91 [36]	76.6 cm^{-1}
IL phantom	~25–675 nm [37]	4.15 cm^{-1}	6.97 cm^{-1}	0.73 [37]	not calculated
PS1 phantom	1.0 μm	4.15 cm^{-1}	6.95 cm^{-1}	0.916 (Mie calc.)	not calculated
PS2 phantom	1.4 μm	4.14 cm^{-1}	6.97 cm^{-1}	0.929 (Mie calc.)	not calculated
PS3 phantom	1.4 μm	4.15 cm^{-1}	5.50 cm^{-1}	0.929 (Mie calc.)	77 cm^{-1}

[a]Mean scatterer diameter (d) of phantoms, absorption coefficient (μ_a), reduced scattering coefficient (μ_s'), anisotropy factor (g) and scattering coefficient (μ_s). μ_a and μ_s' were measured and matched directly; g values were obtained from literature (liver, Intralipid) or calculated from Mie theory (PS samples); μ_a and μ_s were calculated from μ_s' and g where necessary.

#154276 - $15.00 USD Received 7 Sep 2011; revised 5 Oct 2011; accepted 6 Oct 2011; published 4 Nov 2011

After optical properties determination, the liver was cut into approximately 1cm × 1cm × 4cm shapes, and put in quartz cuvette for Mueller matrix measurements. Three different livers obtained from different animals were used, and from each liver three samples were extracted for polarimetric measurements, so a total of nine samples were investigated. To minimize the effect of dehydration, the liver cuvette was covered by a cap, and all the experiments were completed within an hour. The tissue polarimetry experiments were followed by measurements of the IL and PS phantoms. The latter were also repeated three times each to obtain comparable statistics.

3. Results and discussion

We imaged each sample three times, derived the Mueller matrices, decomposed each of the matrices and calculated total, linear and circular depolarizations. Figure 2 shows the spatial maps of the total depolarization Δ_T, linear depolarization Δ_L and circular depolarization Δ_C of

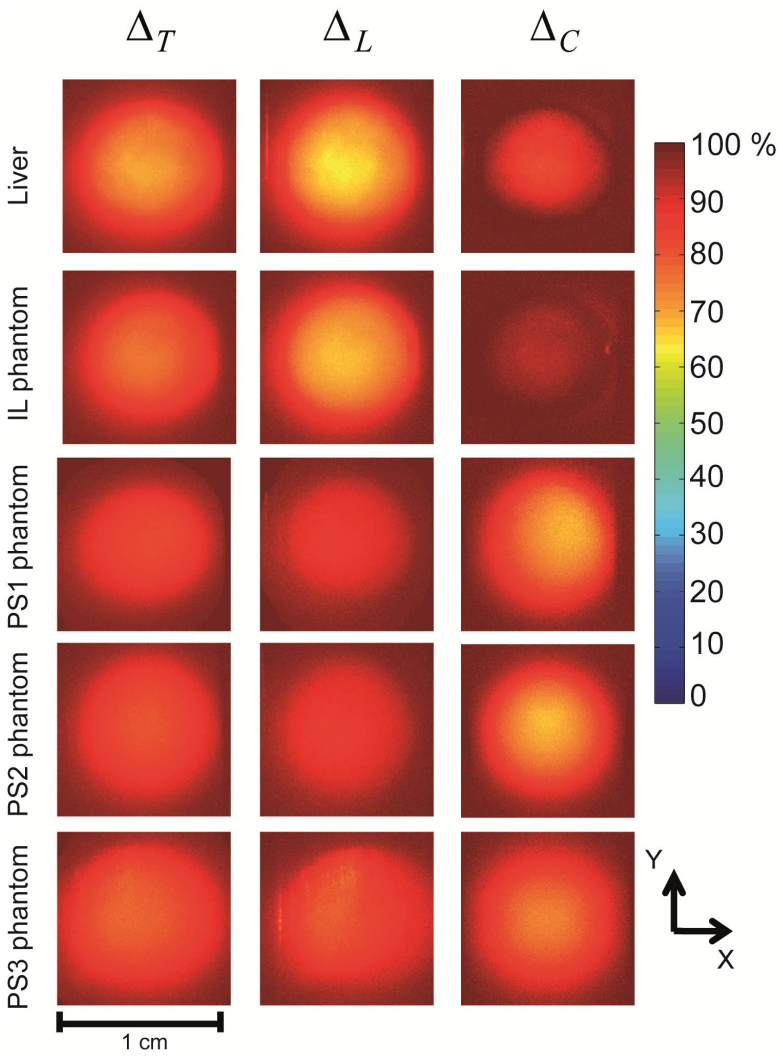

Fig. 2. Total, linear and circular depolarization images of porcine liver and the phantoms derived from Mueller matrix measurements in the backscattering geometry. A 1cm x 1cm field of view for each image is shown. The scale bar indicates depolarization percentage values, with deep red signifying 100% depolarization (complete loss of polarized light information).

#154276 - $15.00 USD Received 7 Sep 2011; revised 5 Oct 2011; accepted 6 Oct 2011; published 4 Nov 2011

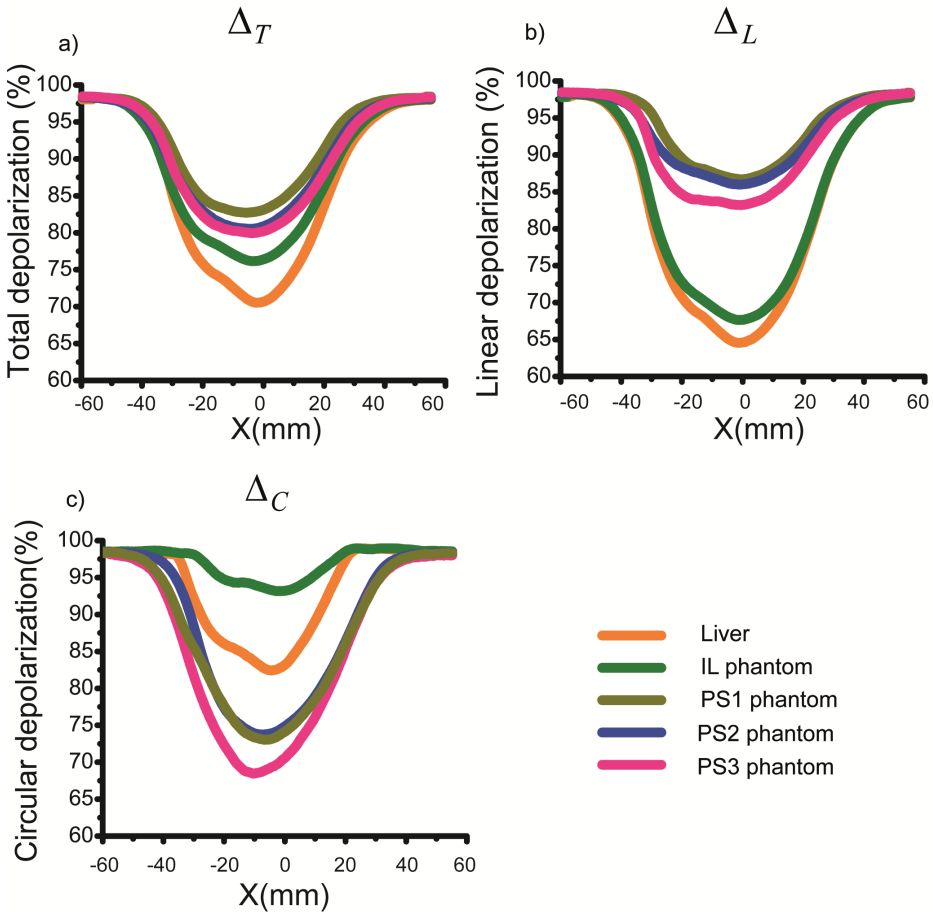

Fig. 3. Representative plots of average total, linear and circular depolarizations. a) total depolarization, b) linear depolarization and c) circular depolarization along x axis in Fig. 2, averaged over the 5-mm ± y central strip . The error bar for all the graphs is 1.5%; this is the standard deviation of the pixel intensities in each image of Fig. 2. The error bar size is equal to the line thickness.

porcine liver and all the phantoms used in this study. The standard deviation of all the pixels in the images among the three measurements was 1.5%; this is representative of the noise level in the system over the measuring period. As seen, typical Δ values for all the samples are in the ~60%-95% range, indicating the highly depolarizing nature of these thick turbid samples measured in the backwards detection geometry. Overall visual comparison of the depolarization images reveals several interesting trends: (i) the Intralipid phantom IL is closest to approximating liver polarimetry results; (ii) the PS phantoms are overall more depolarizing than liver and Intralipid; (iii) linear polarization is better preserved than circular polarization in both liver and Intralipid; (iv) conversely, circular polarization states are better maintained than linear states in all PS phantoms; and (v) the three PS phantoms exhibit generally similar results (with PS3 being closer to liver polarimetry properties), despite differences in scatterer size and concentration.

To quantify the trends noted in Fig. 2, the depolarization values were averaged over 1 mm widths in the y direction and plotted along the x direction of each image displayed in Fig. 2. The trends (i)-(v) seen from the images of Fig. 2 can be discerned more clearly from the resultant plots shown in Fig. 3, and the histogram representation of Fig. 4. We now attempt to explain and interpret these findings.

#154276 - $15.00 USD Received 7 Sep 2011; revised 5 Oct 2011; accepted 6 Oct 2011; published 4 Nov 2011

Polystyrene phantoms consist of discrete monodisperesed spherical particles suspended in water with significant scatterer/background refractive index contrast (~1.59/1.33) while biological tissues, like liver, are random-continuum type of media (connective fibers, cells, nuclei, other cytoplasmic organelles) without distinct optical boundaries and much lower index contrast variations [38]. Intralipid phantoms fall between these two categories since the Intralipid particles are neither spherical nor uniform in size, with intermediate values of index contrast (~1.46/1.33) [37]. Therefore, despite the matched bulk optical properties of the two types of phantoms and of the liver, the individual scatterers' characteristics such as sizes, shapes, refractive index contrast and profiles in each of these samples are very different. We attempt to explain the observed trends (i)-(v) based on the geometry, scatterer size and relative refractive indices; additional effects of the different refractive index profiles (random particulate versus random continua) may also contribute. Scatterers' sizes d, relative refractive indices m and some scattering-related parameters are listed in Table 2. Note that for the liver and IL phantom, the numbers are approximate as taken from literatures. Moreover, the ranges are large; for instance, the liver's scatterers sizes seems to indicate a range of 300 nm-10 μm [39,40]. Schmitt *et al.* have shown that this range can be modeled by an equivalent medium composed of spherical scatterers with a diameter size range ~0.5-1 μm, and we're using this approximation for the purposes of the following discussion [38].

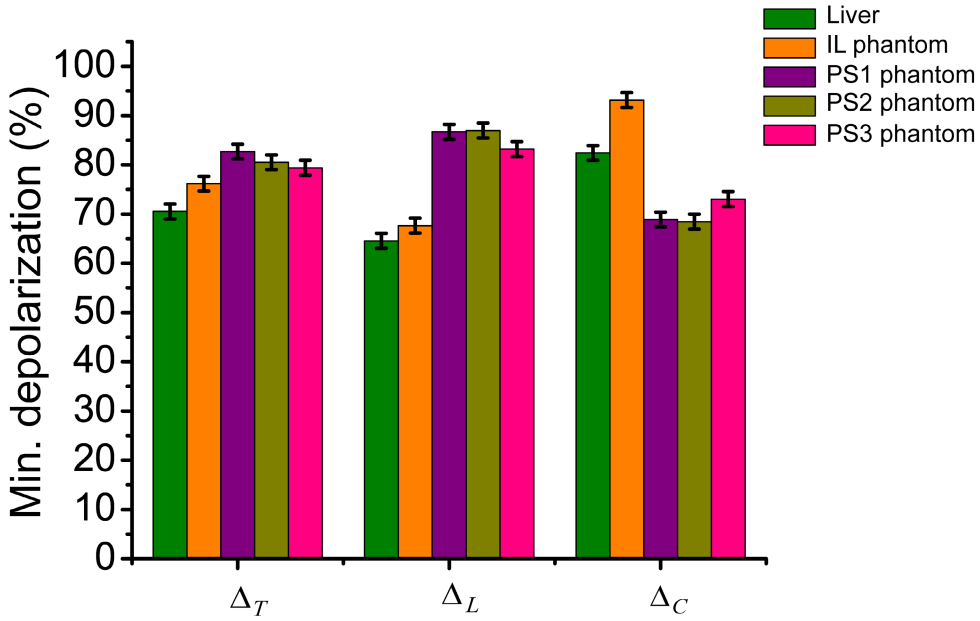

Fig. 4. Percentage values of minimum total (Δ_T), linear (Δ_L), and circular (Δ_C) depolarizations for all samples. The error bars indicate uncertainty (standard deviations) of each measurement.

Table 2. Relevant properties of the liver and its phantoms[a]

Sample	$m = n_{scatt}/n_{back}$	d (μm)	$x = \pi d/\lambda$	$x(m-1)$
Liver	1.04–1.1 [39]	0.5–1 [39,40]	3.25–6.5	0.13–0.65
IL phantom	1.1 [37]	26–675 [37]	0.16–4.4	0.01–0.4
PS phantoms	1.2	1,1.4	6.58, 9.21	1.31, 1.82

[a]m is the relative refractive index of the scatterers with refractive index n_{scatt} compared to the background medium with refractive index n_{back}, d is the diameter of the particles, x is the size parameter $\pi d/\lambda$, where λ is the wavelength of the laser light in the medium, and $x(m-1)$ is the phase shift light experiences when passing through the scatterers.

#154276 - $15.00 USD Received 7 Sep 2011; revised 5 Oct 2011; accepted 6 Oct 2011; published 4 Nov 2011

Based on the values of size parameter x and the relative refractive index m in Table 2, the PS phantoms fall in the Mie scattering regime [41]. In this regime, the scattering is dominated by large particles [39]. Conversely, for IL phantom and liver, the phase shift x(m-1) – that a ray of light experiences upon passing through the scatterer — is smaller than 1, and the value of relative refractive index m is also near unity; these ranges are associated with Rayleigh-Gans scattering regime [39]. This regime behavior is dominated by the small particle scattering (Rayleigh-like scattering) [11,19,40–43]. Trend (i) then makes sense, since liver and IL phantom are in the same category of the scattering regimes (Rayleigh-Gans), different from the Mie-scattering regime of the PS phantoms. Although similar, this does not imply that tissue and Interlipid are identical polarimetrically; note, for example, the better circular polarization preservation for the former relative to the latter. Fine differences in effective scatterer sizes and nature of the refractive index profiles are likely responsible.

Further, comparing the total depolarization minima in Fig. 3(a) and in the left histogram of Fig. 4, liver and IL phantom exhibit less depolarization than the PS phantoms, in the particular backscattering geometry we're reporting here (25° from the backscattering direction). This differs from the previously reported transmission polarimetry results [25]; there, forward transmission through thin samples showed greater tissue depolarization compared to phantoms (both Intralipid and polystyrene). In fact, these differences are not surprising since the single scattering phase functions vary with the scattering regime, and this variation will likely lead to different experimental observables as function of detection geometry. Consider that the Mie scattering phase function associated with the larger scattering particles as present in the PS phantoms is forward peaked with a modest backwards lobe. Conversely, for the smaller sized scatterers in liver and IL phantom, the Rayleigh-Gans phase function is still forward-anisotropic but less so, exhibiting a larger lobe in the backward direction compared to the Mie regime [40–43]. Therefore, photons detected in the backwards directions are more likely to undergo fewer scattering events (and thus be depolarized less) in the Raleigh-Gans (liver, Interlipid) media relative to the Mie (PS phantoms) media. Thus, PS phantoms are more depolarizing in reflection mode as observed in trend (ii); note that this argument does not hold in the forward transmission, where the larger forward anisotropy of the single-scattering Mie phase function is expected to favor polarization preservation for this type of media relative to tissue (as reported previously [25]).

Figure 3 also reports differences in linear versus circular polarization preservations, as summarized in trends (iii) and (iv). To understand this, we again invoke the scattering regimes discussed above. Mie scattering regime is known for better retention of circular polarization, as indeed seen with PS phantoms in Fig. 3(c) and the right histogram of Fig. 4 [41]. On the other hand, Rayleigh-Gans polarization behavior is similar to that in the Rayleigh regime, implying better survival of linear compared to circular states upon scattering [11,16,19]. This is also seen in Fig. 2 and Fig. 3, where liver and IL phantom both show lower linear depolarization as both are categorized in Rayleigh-Gans regime. We emphasize that the reported results are specific to the reflection imaging geometry from the thick (1cm) samples.

Finally, it's illustrative to compare PS3 depolarization behavior with PS1 and PS2, as noted in trend (v). As Fig. 3 and Fig. 4 show, PS3 approximates the polarization behavior of liver somewhat better than do the PS phantoms 1 and 2 (although not as accurately as the Interlipid phantom). It thus appears that matching the scattering coefficient (PS3) results in a better polarimetric tissue approximation than matching the reduced scattering coefficient (PS1 and PS2). Also, 30% change in the scatterer diameter from PS1 to PS2 did not translate into a significant change in the depolarization behavior since both sizes are still 'large' in the sense of Mie scattering. Overall though, PS phantoms are poor candidates for modeling tissue polarimetric behavior in reflection geometries (as well as in other directions, revealed via additional experiments (data not shown)).

#154276 - $15.00 USD Received 7 Sep 2011; revised 5 Oct 2011; accepted 6 Oct 2011; published 4 Nov 2011

4. Conclusion

In this study, we have studies polarized light propagation in porcine liver, polystyrene and Intralipid phantoms with liver-matched bulk optical properties. Significant polarimetric differences between liver and its phantoms were observed in the thick-sample reflection geometry. The results show that all the phantoms are more depolarizing than liver, which is contrary to previously reported results in transmission mode. Generally, our results show that as compared to PS phantoms, IL phantom depolarization rates are closer to the liver. Both liver and IL phantoms exhibit better retention of linear polarization as compared to circular light, while PS phantoms have better retention of circular light as compared to linear. It is also noted that PS3 (with μ_s matched) exhibits somewhat closer polarization behavior to liver than the PS1 & PS2 (with μ_s' matched), but not as close as IL phantom. These finding are qualitatively consistent with the Rayleigh-Gans and Mie scattering regimes, with their associated differences in the single-scattering phase functions. Overall, our results demonstrate that matching bulk optical properties between tissue and its various simulating phantoms does not ensure similar polarimetric behavior, and care must be taken in proper polarimetric phantom design. Insights gained from the current study will be useful for further advances in tissue polarimetry (e.g., linear polarimetric examination of tissues in the backwards direction is more promising than its thin-slab transmission counterpart).

Acknowledgments

This work was supported by the Natural Sciences and Engineering Research Council of Canada. Manzoor Ahmad acknowledges the Higher Education Commission (HEC), Islamabad, Pakistan for the financial support through the Indigenous Fellowship Scheme for Ph.D. studies.

#154276 - $15.00 USD Received 7 Sep 2011; revised 5 Oct 2011; accepted 6 Oct 2011; published 4 Nov 2011